The Astrophysical Journal, 887:116 (8pp), 2019 December 20 https://doi.org/10.3847/1538-4357/ab528c

Compressible and Incompressible Magnetic Turbulence Observed in the Very Local Interstellar Medium by *Voyager 1*

G. P. Zank[1,2], M. Nakanotani[1], and G. M. Webb[1]
[1] Center for Space Plasma and Aeronomic Research (CSPAR), University of Alabama in Huntsville, Huntsville, AL 35805, USA
[2] Department of Space Science, University of Alabama in Huntsville, Huntsville, AL 35899, USA
Received 2019 August 22; revised 2019 October 14; accepted 2019 October 28; published 2019 December 16

Abstract

Voyager 1 observed Kolmogorov-like ($k^{-5/3}$) compressible turbulence just upwind of the heliopause. Subsequent measurements by *Voyager 1* further from the heliopause revealed that the observed fluctuations were now fully incompressible, with a $k^{-5/3}$ spectrum that was essentially identical to that of the earlier compressible spectrum. Zank et al. showed that only compressible fast magnetosonic modes could be transmitted from the inner heliosheath into the very local interstellar medium (VLISM), and could exhibit a $k^{-5/3}$ spectrum. We show here that the small plasma beta VLISM admits three-wave interactions between a fast magnetosonic mode, a zero-frequency mode, and an Alfvén wave. The fast magnetosonic mode is converted to an incompressible Alfvén (or zero-frequency) mode with wavenumber almost identical to that of the initial compressible fast mode. The initial compressible and generated incompressible spectra are essentially identical. For the wavelength range observed by *Voyager 1*, we estimate that compressible fast modes are fully mode-converted to incompressible fluctuations within ∼10 au of the heliopause. We suggest that the VLISM magnetic field spectrum is a superposition of a higher amplitude $\sim k^{-5/3}$ spectrum of heliospheric origin with an estimated correlation length ∼30 au, having a minimum wavenumber $\sim(100)^{-1}$ $(\mathrm{au})^{-1}$, and a lower amplitude (possibly local) ISM $k^{-5/3}$ spectrum, the latter possessing an outer scale $\geqslant 2$ pc. We suggest that the transmission of compressible turbulence from an inner asterosheath into the local circumstellar interstellar medium surrounding a star, and the subsequent mode conversion to incompressible turbulence, may be a general mechanism by which stars drive turbulence in the interstellar medium.

Unified Astronomy Thesaurus concepts: Interstellar magnetic fields (845); Interplanetary turbulence (830); Heliopause (707)

1. Introduction

The observation by *Voyager 1* of compressible turbulence exhibiting a Kolmogorov-like spectrum in the very local interstellar medium (VLISM[3]), as reported by Burlaga et al. (2015), was rather unexpected. Interstellar turbulence dominated by compressible fluctuations has potentially important implications for our understanding of turbulence processes throughout the interstellar medium and for cosmic-ray propagation in particular (Zank et al. 2017b). The *Voyager 1* magnetometer observations showed that interstellar magnetic field fluctuations over the frequency range $\sim 5.57 \times 10^{-6}$ Hz to 2.47×10^{-8} Hz were largely compressive, i.e., the observed magnetic field fluctuations possessed a primarily $\delta B_{\parallel}$ component parallel to the mean or ambient interstellar magnetic field, with very little or negligible contribution from transverse magnetic field fluctuations. Such fluctuations are characteristic of magnetosonic modes for which $\delta B_{\parallel} \neq 0$ and the transverse magnetic field fluctuations $\delta \boldsymbol{B}_{\perp} = 0$. These observations were made during a quiet interval between 2013.3593 and 2014.6373 (i.e., between a heliocentric distance of 124.391603 and 129.475722 au), called Interval 1 in the nomenclature of Burlaga et al. (2018). No interstellar shocks were present during Interval 1. Furthermore, the power spectral density (PSD) of the compressible fluctuations was a Kolmogorov-like spectrum with a $\sim k^{-5/3}$ power law in wavenumber k (Burlaga et al. 2015, 2018). Lee & Lee (2019) find a possibly related spectrum for electron density fluctuations observed by the *Voyager 1* plasma wave instrument (Gurnett et al. 2013).

It came as a further surprise when Burlaga et al. (2018) subsequently reported that magnetic fluctuations observed in a later quiet interval, Interval 2, of VLISM plasma between 2015.3987 and 2016.6759 (located between heliocentric distances of 131.623998 and 136.948596 au) were now fully incompressible and dominated by transverse fluctuations, i.e., $\delta B_{\parallel} = 0$ and $\delta \boldsymbol{B}_{\perp} \neq 0$, over the same frequency range. Interval 2 is obviously further from the heliopause (located at ∼121.6 au[4]) than was Interval 1. Furthermore, as illustrated in Figure 4 of Burlaga et al. (2018), the amplitude of the PSDs over the wavenumber range $\sim 1.3 \times 10^{-13}$–$\sim 4 \times 10^{-12}$ cm^{-1} for Intervals 1 and 2 was essentially identical. In other words, the dominant component of the turbulence during Interval 1 had magnetic fluctuations aligned with the VLISM mean magnetic field (i.e., compressible turbulence comprised of magnetosonic modes), whereas the dominant component of the turbulence during Interval 2 had magnetic fluctuations transverse to the VLISM

[3] Here we use the definition introduced by Zank (2015) and Zank et al. (2017b), which is that the VLISM is "that region of the interstellar medium surrounding the Sun that is modified or mediated by heliospheric processes or material."

[4] There is little reason to suppose this distance to the heliopause is fixed since it is expected to move inward or outward in response to the solar cycle, collisions with interplanetary shocks (Zank & Müller 2003; Washimi et al. 2017), and the intrinsic (in)stability of the heliopause (Zank 1999b; Florinski et al. 2005; Borovikov et al. 2008; Avinash et al. 2014; Borovikov & Pogorelov 2014). The distance from the heliopause to Intervals 1 and 2 is therefore somewhat uncertain.

mean magnetic field (i.e., incompressible turbulence comprised of Alfvén waves and/or non-propagating or zero-frequency quasi-2D structures in a plane orthogonal to the mean magnetic field). As emphasized by Burlaga et al. (2018), in view of the uncertainties in the measurements, it is important to verify these results with further observations from *Voyagers 1* and *2*. For the present, "if the apparent transformation (from compressible to incompressible turbulence) was a physical effect, …, it is necessary to determine the nature and production mechanism of the transverse component of the turbulence (Burlaga et al. 2018)."

In this note, we provide a physical explanation for the apparent transformation of turbulence from compressible to incompressible and why the amplitude, slope, and wavenumber range of the PSD do not change from Interval 1 to Interval 2.

Three points are important to bear in mind about the VLISM plasma:

1. the inner heliosheath (the region between the heliospheric termination shock and heliopause—see Zank (1999a), Zank (2015) for a general overview of the interaction of the heliosphere with the interstellar medium) exhibits high levels of compressible turbulence (Burlaga et al. 2006; Fraternale et al. 2019);
2. the VLISM is a small plasma beta β_p environment ($\beta_p = P/(B^2/2\mu_0)$, where P is the thermal gas pressure, $B = |\boldsymbol{B}|$ is the magnetic field strength, and μ_0 is the permeability of free space) with β_p ranging from 0.1 to 0.4 (Zank et al. 2017b) depending on whether one assumes a VLISM temperature in the range of ∼6500 K to ∼20,000 K, and
3. the VLISM flow toward and around the heliopause is sub-fast magnetosonic, either by virtue of the presence of a bow shock/wave (Zank et al. 2013; Pogorelov et al. 2017) or because the LISM is intrinsically subsonic (Zank et al. 2013, 1996).

From points (1) and (2) above, Zank et al. (2017b) showed that only fast magnetosonic modes can be transmitted from the inner heliosheath, across the heliopause, and into the VLISM. Neither Alfvén waves nor slow magnetosonic modes can be transmitted from the inner heliosheath into the VLISM. The analysis of Zank et al. (2017b) has since been confirmed by Matsukiyo et al. (2019) using PIC simulations of a VLISM-solar wind "shock tube problem." The PIC simulations showed that only fast magnetosonic modes were transmitted into the VLISM from the inner heliosheath. If the fast mode compressible component in the inner heliosheath possessed a Kolmogorov-like PSD, then the spectrum in the VLISM was shown to be Kolmogorov-like too. Point (3) indicates that fast magnetosonic waves can propagate further into the VLISM, hence the puzzle identified by Burlaga et al. (2018) is why are these modes not seen in Interval 2? The answer to this question, as we show below, is that the fast magnetosonic waves undergo mode conversion via a three-wave interaction as they propagate in the approximately homogeneous VLISM, decaying into an Alfvén wave and a zero-frequency Elsässer vortex, both of which possess only a transverse magnetic field component $\delta\boldsymbol{B}_\perp$.

Fraternale et al. (2019) have further investigated low-frequency turbulence in both the inner heliosheath and VLISM using a combination of *Voyager 1* and 2 magnetometer and plasma data for the inner heliosheath and *Voyager 1* data for the VLISM. Their results both complement and extend the previous results and conclusions of Burlaga et al. (2015, 2018). Fraternale et al. (2019) find that turbulence in the inner heliosheath is highly compressive, extending the Burlaga et al. (2006) analysis to five frequency decades. Similarly, Fraternale et al. (2019) extended the frequency range of the Burlaga et al. (2015, 2018) VLISM analysis and examined two additional intervals. They found that after 2015 May the magnetic field fluctuations were predominantly transverse in character. Although not discussed here, Fraternale et al. (2019) found evidence for intermittency only on scales smaller than 10^{-6} Hz. Fraternale et al. (2019) try to assess the spectral compressibility of the VLISM fluctuations in Intervals 1 and 2 by plotting the PSD($|\boldsymbol{B}|$)$/E_m$, where E_m is defined in terms of the trace of the PSD of $\boldsymbol{B}$. Fraternale et al. suggest using this as a proxy in the absence of VLSIM plasma data because, in the supersonic solar wind, Roberts et al. (1987) find a strong correlation between magnetic field and density fluctuations in compression and rarefaction regions between 1 and 11 au. The strength of the correlation relies on the fluctuations (fields and plasma) being essentially incompressible, which is typically reasonable in the supersonic solar wind. Given that the VLSIM fluctuations over the range of scales of interest were dominated initially by highly compressible wave fluctuations (fast magnetosonic waves probably), such a correlation between density and magnetic field fluctuations may not be completely reliable. At this point, we simply do not know whether higher frequencies are indeed more compressible and this will need to be re-examined using *Voyager 2* VLISM observations.

In the following section, we formulate the problem in the context of a nearly incompressible magnetohydrodynamic (NI MHD) description. The approach is novel in that it allows for a clean distinction between non-propagating modes and slow magnetosonic modes in the small plasma beta limit. NI MHD therefore lends itself to the investigation of nonlinear wave interactions, and the identification of the relevant mode couplings in the $\beta_p \ll 1$ VLISM. Based on the *Voyager 1* observations, we cannot determine yet for certain whether the VLISM is nearly incompressible, one of the criteria being that the turbulent sonic Mach number of the fluctuations be small (below), since *Voyager 1* does not have a working plasma instrument. However, the remarkable quiescence of the magnetic field fluctuations may hint that corresponding velocity fluctuations are similarly quiescent. We will accordingly assume that the VLISM is weakly compressible. In the final section, besides summarizing our results, we discuss briefly the implications of the characteristics of turbulence in the VLISM (compressibility and mode conversion) for turbulence in the general ISM.

2. Nonlinear Mode Interactions in an NI MHD Framework

As we illustrate below, the formulation of NI MHD lends itself ideally to the investigation of the nonlinear coupling of low-frequency fluctuations in a plasma (see e.g., Webb et al. 1999, 2000, 2001; Galtier et al. 2001; Kuznetsov 2001, and references therein for more general treatments). Based on the initial formulation (Zank & Matthaeus 1992a, 1992b, 1993; Hunana & Zank 2010), Zank et al. (2017a) developed the theory of NI MHD turbulence that we use here. NI MHD describes a magnetofluid that is in a state of weak compressibility due to conditions that allow a fully compressible fluid to converge to the corresponding incompressible fluid in the limit that the "turbulent" Mach number, suitably

defined, approaches zero (Klainerman & Majda 1981, 1982; Zank & Matthaeus 1992a, 1992b, 1993; Hunana & Zank 2010). Because of the relationship of the turbulent Alfvén Mach number to the plasma beta, the leading-order incompressible descriptions for the $\beta_p \gg 1$ and $\beta_p \sim 1$ and $\ll 1$ regimes are quite different. It is the latter case that is of interest to the VLISM. In the $\beta_p \ll 1$ regime, the leading-order incompressible MHD description is 2D with respect to a plane perpendicular to the mean magnetic field, and the nearly incompressible contributions comprise 3D compressible propagating modes and Alfvén modes propagating along the mean magnetic field. Thus, Zank & Matthaeus (1992b, 1993) predicted that turbulence in the $\beta_p \ll 1$ (and ~ 1) regime should be a superposition of quasi-2D and slab turbulence, dominated by the majority 2D component. Observational support for a 2D-slab superposition model of turbulence in the solar wind has accumulated (e.g., Matthaeus et al. 1991; Bieber et al. 1994, 1996; Zhou et al. 2004; Alexandrova 2008; Telloni et al. 2013; Khabarova et al. 2015a, 2015b, 2016, 2017; Lion et al. 2016; Perrone et al. 2016, 2017; Adhikari et al. 2017a, 2017b, 2019; Khabarova & Zank 2017; Zank et al. 2018; Zhao et al. 2018a, 2018b, 2019).

The $\beta_p \ll 1$ NI MHD equations may be expressed as a majority 2D incompressible component and a minority nearly incompressible component. We use the superscript "∞" to denote 2D component variables such as the flow velocity $\boldsymbol{u}^\infty$, magnetic field $\boldsymbol{B}^\infty$, and pressure P^∞, and we use $\nabla_\perp \equiv (\partial_x, \partial_y, 0)$, where a mean magnetic field $\boldsymbol{B}_0$ defines the parallel direction. The majority incompressible component satisfies the standard incompressible 2D MHD equations where the orientation is in a plane perpendicular to the mean magnetic field, hence (Zank et al. 2017a),

$$\frac{\partial \boldsymbol{u}^\infty}{\partial t} + \boldsymbol{u}^\infty \cdot \nabla_\perp \boldsymbol{u}^\infty = -\frac{1}{\rho_0}\nabla_\perp\left(P^\infty + \frac{B^{\infty 2}}{2\mu_0}\right) + \frac{1}{\mu_0 \rho}\boldsymbol{B}^\infty \cdot \nabla_\perp \boldsymbol{B}^\infty; \quad (1)$$

$$\frac{\partial \boldsymbol{B}^\infty}{\partial t} + \boldsymbol{u}^\infty \cdot \nabla_\perp \boldsymbol{B}^\infty = \boldsymbol{B}^\infty \cdot \nabla_\perp \boldsymbol{u}^\infty; \quad (2)$$

$$\nabla_\perp \cdot \boldsymbol{u}^\infty = 0; \qquad \nabla_\perp \cdot \boldsymbol{B}^\infty = 0, \quad (3)$$

and ρ_0 is the mean background density. On introducing the 2D Elsässer variables

$$z^{\infty\pm} = \boldsymbol{u}^\infty \pm \frac{\boldsymbol{B}^\infty}{\sqrt{\mu_0 \rho_0}}, \quad (4)$$

Equations (1)–(3) are expressed conveniently as

$$\frac{\partial z^{\infty\pm}}{\partial t} + z^{\infty\mp} \cdot \nabla_\perp z^{\infty\pm} = -\frac{1}{\rho_0}\nabla_\perp\left(P^\infty + \frac{B^{\infty 2}}{2\mu_0}\right); \quad \nabla_\perp \cdot z^{\infty\pm} = 0. \quad (5)$$

Notice in Equations (1)–(3) and (5) that Alfvén wave propagation effects are absent and that only non-propagating structures such as vortices are admissible solutions (e.g., Kadomtsev & Pogutse 1973; Verkhoglyadova et al. 2003; Alexandrova 2008; Zank et al. 2017a).

Propagation effects enter the nearly incompressible equations. We now use the superscript "*" to identify the NI component variables, i.e., density ρ^*, velocity $\boldsymbol{u}^*$ (in previous NI MHD papers, the NI velocity was denoted by $\boldsymbol{u}_1$), thermal pressure P^*, and magnetic field $\boldsymbol{B}^*$. The NI equations are fully 3D and given by (Zank et al. 2017a)

$$\frac{\partial \rho^*}{\partial t} + \boldsymbol{u}^\infty \cdot \nabla \rho^* + \rho_0 \nabla \cdot \boldsymbol{u}^* = 0; \quad (6)$$

$$\frac{\partial \boldsymbol{u}^*}{\partial t} + \boldsymbol{u}^\infty \cdot \nabla \boldsymbol{u}^* + \boldsymbol{u}^* \cdot \nabla \boldsymbol{u}^\infty = -\frac{1}{\rho_0}\nabla P^* - \frac{1}{\mu_0 \rho_0}\nabla(\boldsymbol{B}_0 \cdot \boldsymbol{B}^* + \boldsymbol{B}^\infty \cdot \boldsymbol{B}^*) + \frac{1}{\mu_0 \rho_0}(\boldsymbol{B}_0 + \boldsymbol{B}^\infty) \cdot \nabla \boldsymbol{B}^* + \frac{1}{\mu_0 \rho_0}\boldsymbol{B}^* \cdot \nabla \boldsymbol{B}^\infty; \quad (7)$$

$$\frac{\partial P^*}{\partial t} + \boldsymbol{u}^\infty \cdot \nabla P^* + \gamma P_0 \nabla \cdot \boldsymbol{u}^* = -\frac{\partial P^\infty}{\partial t} - \boldsymbol{u}^\infty \cdot \nabla P^\infty; \quad (8)$$

$$\frac{\partial \boldsymbol{B}^*}{\partial t} + \boldsymbol{u}^\infty \cdot \nabla \boldsymbol{B}^* - \boldsymbol{B}^* \cdot \nabla \boldsymbol{u}^\infty = (\boldsymbol{B}_0 + \boldsymbol{B}^\infty) \cdot \nabla \boldsymbol{u}^* - (\boldsymbol{B}_0 + \boldsymbol{B}^\infty)\nabla \cdot \boldsymbol{u}^* - \boldsymbol{u}^* \cdot \nabla \boldsymbol{B}^\infty; \quad (9)$$

$$\nabla \cdot \boldsymbol{B}^* = 0. \quad (10)$$

By introducing the NI Elsässer variables,

$$z^{*\pm} = \boldsymbol{u}^* \pm \frac{\boldsymbol{B}^*}{\sqrt{\mu_0 \rho_0}}. \quad (11)$$

Equations (6)–(10) can be expressed in a convenient form as (Zank et al. 2017a)

$$\frac{\partial z^{*\pm}}{\partial t} \mp \boldsymbol{V}_{A0} \cdot \nabla z^{*\pm} + z^{\infty\mp} \cdot \nabla z^{*\pm} + z^{*\mp} \cdot \nabla z^{\infty\pm} = -\frac{1}{\rho_0}\nabla\left(P^* + \frac{1}{\mu_0}\boldsymbol{B}_0 \cdot \boldsymbol{B}^* + \frac{1}{\mu_0}\boldsymbol{B}^\infty \cdot \boldsymbol{B}^*\right) \mp \left(\boldsymbol{V}_{A0} + \frac{\boldsymbol{B}^\infty}{\sqrt{\mu_0 \rho_0}}\right)\nabla \cdot \boldsymbol{u}^*, \quad (12)$$

which clearly shows the presence of propagation effects through the Alfvén velocity $\boldsymbol{V}_{A0} = \boldsymbol{B}_0/\sqrt{\mu_0 \rho_0}$. The source terms in Equation (8) have been neglected—see Zank et al. (2017a) for further discussion. Also noticeable is the interaction of the NI $z^{*\pm}$ modes with the incompressible quasi-2D structures $z^{\infty\mp}$. This results in the scattering and mixing (and coupling) of NI modes through collisions with non-propagating 2D modes. It is useful to consider the higher-order generalization of the Elsässer transport Equation (12) that includes the nonlinear term $z^{*\mp} \cdot \nabla z^{*\pm}$, derived in Zank et al. (2017a),

$$\frac{\partial z^{*\pm}}{\partial t} \mp \boldsymbol{V}_{A0} \cdot \nabla z^{*\pm} + z^{\infty\mp} \cdot \nabla z^{*\pm} + z^{*\mp} \cdot \nabla z^{\infty\pm} + z^{*\mp} \cdot \nabla z^{*\pm} = -\frac{1}{\rho_0}\nabla\left(P^* + \frac{1}{\mu_0}\boldsymbol{B}_0 \cdot \boldsymbol{B}^* + \frac{1}{\mu_0}\boldsymbol{B}^\infty \cdot \boldsymbol{B}^*\right) \mp \left(\boldsymbol{V}_{A0} + \frac{\boldsymbol{B}^\infty}{\sqrt{\mu_0 \rho_0}}\right)\nabla \cdot \boldsymbol{u}^*. \quad (13)$$

Although we discuss this further below, we remark that (13) can be decomposed into an equation describing incompressible modes ($\nabla \cdot \boldsymbol{u}^* = 0$) and another describing compressible modes

$(\nabla \cdot \boldsymbol{u}^* \neq 0)$. The gradient operator ∇ in Equations (6)–(13) is 3D.

Since we consider the nonlinear coupling of linear modes below, we discuss briefly the linear wave modes admitted through the Elsässer formulation of NI MHD, i.e., we neglect the various nonlinear terms in (5) and (13).

On introducing the Elsässer vorticity (the sum and difference of the fluid vorticity and the current density),

$$\eta^{\infty\pm} = \nabla_\perp \times \boldsymbol{z}^{\infty\pm}, \tag{14}$$

Equation (5) becomes as usual

$$\frac{\partial \eta^{\infty\pm}}{\partial t} + \boldsymbol{z}^{\infty\mp} \cdot \nabla \eta^{\infty\pm} = 0. \tag{15}$$

The neglect of the nonlinear terms yields zero-frequency ($\omega = 0$) modes satisfying

$$\boldsymbol{z}^{\infty\pm} = \hat{z}^{\infty\pm}(-\cos\theta, \sin\theta), \tag{16}$$

where θ is the angle between the $\boldsymbol{k}_\perp$ vector and the x-direction and $\hat{z}^{\infty\pm} = |\boldsymbol{z}^{\infty\pm}|$. Thus, by analogy with incompressible fluid dynamics, the $\boldsymbol{z}^{\infty\pm}$ are vortices in the 2D plane orthogonal to the mean magnetic field, and energy transfer proceeds through the nonlinear coupling of Elsässer vortical fluctuations $\boldsymbol{z}^{\infty\pm}$ at the nonlinear timescale.

Consider now the Elsässer transport Equation (13) for the NI component. Two cases need to be considered; the incompressible with $\nabla \cdot \boldsymbol{u}^* = 0$ and the compressible with $\nabla \cdot \boldsymbol{u}^* \neq 0$. We neglect the nonlinear terms and assume first that $\nabla \cdot \boldsymbol{u}^* = 0$. The latter condition shows that P^* and ρ^* are zero. Since $\boldsymbol{B}_0 = B_0\hat{z}$ defines the parallel direction, Equations (8) and (9) show that $u_z^* = 0 = B_z^*$. Equation (13) then reduces to the transport equation for Alfvén waves propagating parallel and anti-parallel to the mean magnetic field, i.e.,

$$\frac{\partial \boldsymbol{z}^{*\pm}}{\partial t} = \pm \boldsymbol{V}_{A0} \cdot \nabla \boldsymbol{z}^{*\pm}, \tag{17}$$

which, on assuming $\boldsymbol{z}^{*\pm} = \hat{\boldsymbol{z}}^{*\pm} \exp[i(\boldsymbol{k} \cdot \boldsymbol{x} - \omega t)]$, yields the Alfvén dispersion relation for the frequency ω and wavenumber $\boldsymbol{k}$

$$\omega = \mp \boldsymbol{V}_{A0} \cdot \boldsymbol{k}. \tag{18}$$

Consider now $\Delta \equiv \nabla \cdot \boldsymbol{u}^* = \nabla \cdot \boldsymbol{z}^{*\pm} \neq 0$ and neglect the nonlinear terms in (13). A little algebra yields the wave equation (Lighthill 1960; Zank et al. 2017a)

$$\frac{\partial^2 \Delta}{\partial t^2} - C_{s0}^2 \nabla^2 \Delta = V_{A0}^2 \nabla^2 (\Delta - \Gamma), \tag{19}$$

where $\Gamma = \partial u_z^*/\partial z$ and $C_{s0}^2 = \gamma P_0/\rho_0$ is the square of the sound speed. Equation (19) can be further factored using (7) to give the wave equation for fast and slow magnetosonic modes

$$\frac{\partial^4 \Delta}{\partial t^4} - (V_{A0}^2 + C_{s0}^2)\nabla^2 \frac{\partial^2 \Delta}{\partial t^2} + V_{A0}^2 C_{s0}^2 \nabla^2 \frac{\partial^2 \Delta}{\partial z^2} = 0, \tag{20}$$

which, for $\Delta \propto \exp[i(\boldsymbol{k} \cdot \boldsymbol{x} - \omega t)]$ yields the dispersion relation

$$\omega^4 - (V_{A0}^2 + C_{s0}^2)\omega^2 k^2 + V_{A0}^2 C_{s0}^2 k^4 \cos^2\theta = 0, \tag{21}$$

and θ is the angle between $\boldsymbol{k}$ and the mean magnetic field direction, and $k = |\boldsymbol{k}|$. We will need the following results. For propagation parallel ($\theta = 0$) and perpendicular ($\theta = \pi/2$) to the mean magnetic field, (21) shows that the fast and slow magnetosonic modes become

$$\omega_{f,s}^2 = V_{A0}^2 k^2,\ C_{s0}^2 k^2 \quad \text{and} \quad (V_{A0}^2 + C_{s0}^2)k^2,\ 0, \tag{22}$$

respectively. In the plasma beta limit $\beta_p \ll 1$, the fast and slow modes are expressed approximately as

$$\omega_f = \pm V_{A0}\left(1 + \frac{\gamma}{4}\beta_p \sin^2\theta\right)k \quad \text{and}$$
$$\omega_s = \pm V_{A0}\sqrt{\frac{\gamma}{2}\beta_p}\cos\theta k, \tag{23}$$

respectively, i.e., the fast mode propagates at approximately the Alfvén speed V_{A0} and the slow mode at a fraction of that in the small plasma beta limit.

Consider now the effect of the nonlinear terms in Equation (13) on the propagation of fast mode waves. Suppose we have a background of fast mode waves each satisfying $\omega = \pm V_f k$, where V_f is the phase speed of the fast mode, so that

$$\boldsymbol{z}^{*\pm} = \sum_{\boldsymbol{l}} \hat{\boldsymbol{z}}^{*\pm} e^{i(\boldsymbol{l}\cdot\boldsymbol{x} - \omega t)}, \quad \omega = \pm V_f l. \tag{24}$$

The nonlinear terms such as, e.g., $\boldsymbol{z}^{\infty\mp} \cdot \nabla \boldsymbol{z}^{*\pm}$ can therefore be expressed as

$$\sum_{\boldsymbol{k}_\perp} \hat{\boldsymbol{z}}^{\infty\mp} e^{i\boldsymbol{k}_\perp \cdot \boldsymbol{x}} \cdot \nabla \left(\sum_{\boldsymbol{l}} \hat{\boldsymbol{z}}^{*\pm} e^{i(\boldsymbol{l}\cdot\boldsymbol{x} - \omega t)} \right), \tag{25}$$

where the sum over $\boldsymbol{k}_\perp$ refers to zero-frequency 2D fluctuations satisfying the majority 2D component described by Equations (5). The linear part of Equation (13) can support a wave of either the fast, slow, or Alfvénic kind $\propto \exp[i(\boldsymbol{m} \cdot \boldsymbol{x} - \omega''' t)]$ provided the resonance (Manley-Rowe) conditions

$$\boldsymbol{m} = \boldsymbol{k}_\perp + \boldsymbol{l}; \qquad \omega'''(\boldsymbol{m}) = \omega(\boldsymbol{l}), \tag{26}$$

hold. Inspection shows that only two cases are possible. The first is that a fast mode plus a zero-frequency mode generates a slow mode wave since (26) yields $V_s m = V_f\, l$ ($V_s < V_f$ and $V_s \neq 0$ unless $\theta = \pi/2$). This requires that $m > l$ and, since $m^2 = k_\perp^2 + 2\boldsymbol{k}_\perp \cdot \boldsymbol{l} + l^2 = (V_f/V_s)^2 l^2 > l^2$, $k_\perp$ has to satisfy $k_\perp^\pm = -l\cos\phi \pm l\sqrt{(V_f/V_s)^2 - 1 + \cos^2\phi}$, where ϕ is the angle between $\boldsymbol{l}$ and $\boldsymbol{k}_\perp$, i.e., $\boldsymbol{l} \cdot \boldsymbol{k}_\perp = l k_\perp \cos\phi$. However, for the problem of the VLISM with $\beta_p \ll 1$, the condition $V_f/V_s \propto \beta_p^{-1/2} \gg 1$ shows that m is much larger than l and requires $k_\perp$ to be large. In this case, the three-wave interaction involving a fast mode wave with wavenumber l will map to a slow mode wave with wavenumber $m \gg l$. Although slow mode waves do not possess transverse magnetic field fluctuations, and the new slow mode wavenumber spectrum will not coincide with the initial fast mode wavenumber spectrum, it is possible that this particular resonant mode interaction will be important in addressing the high-frequency compressibility that may have been observed by Fraternale et al. (2019). This is discussed further in the conclusions below.

The second possibility is that a fast mode plus a zero-frequency mode generates an Alfvén mode. In this case, Equation (26) yields $\boldsymbol{V}_{A0} \cdot \boldsymbol{m} = V_f l$ or $V_{A0} m_\parallel = V_f l$. For parallel propagating fast magnetosonic modes $V_f = V_{A0}$ and more generally in the VLISM with $\beta_p \ll 1$, $V_f \simeq V_{A0}$ for arbitrary

propagation angles. Hence, $m_{\parallel} \simeq l$ and $m_{\perp}^2 = k_{\perp}^2 + 2\boldsymbol{k}_{\perp} \cdot \boldsymbol{l}$. The interaction of an arbitrarily obliquely propagating fast mode wave with a zero-frequency 2D mode therefore generates an Alfvén wave in the $\beta_p \ll 1$ VLISM.

Corresponding reasoning shows that the nonlinear term $z^{*\mp} \cdot \nabla z^{*\pm}$ allows for a three-wave interaction that generates either an Alfvén wave or a slow mode wave from the interaction of an oblique fast mode with a zero-frequency 2D mode in the $\beta_p \ll 1$ VLISM. In this case, the nonlinear term can be expressed as

$$\sum_{\boldsymbol{k}_{\perp}} \hat{\boldsymbol{z}}^{*\mp} e^{i\boldsymbol{k}\cdot\boldsymbol{x}-\omega' t} \cdot \nabla \left(\sum_{\boldsymbol{l}} \hat{\boldsymbol{z}}^{*\pm} e^{i(\boldsymbol{l}\cdot\boldsymbol{x}-\omega'' t)} \right), \tag{27}$$

and the resonance conditions are now

$$\boldsymbol{m} = \boldsymbol{k} + \boldsymbol{l}; \qquad \omega'''' = \omega' + \omega''. \tag{28}$$

Admissible wave modes are the fast and slow magnetosonic modes and the Alfvén mode. Precisely the same reasoning as above shows that (27) admits a three-wave interaction for a fast, slow, and zero-frequency mode with the same condition that $m \gg l$. Similarly, a three-wave interaction between an Alfvén wave, a fast mode wave (for all propagation angles), and a zero-frequency mode exists. We note that the familiar three-wave interaction between counter-propagating Alfvén waves and a zero-frequency mode is also admitted in the NI MHD framework (see the derivation in Zank et al. 2017a that reflects that given by Shebalin et al. 1983). The remaining nonlinear term with $z^{\infty\pm}$ does not admit a resonant interaction.

Of note is that the three-wave interaction of fast mode plus zero-frequency mode and Alfvén wave replaces the compressible mode (with fluctuations $\delta B_{\parallel} \neq 0$ aligned with the mean magnetic field) of wavenumber k with an incompressible mode (with fluctuations $\delta B_{\perp} \neq 0$ transverse to the mean magnetic field only) with essentially the same wavenumber k. Consequently, the spectrum for the incompressible fluctuations is virtually identical in amplitude and spectral (k) range to the initial compressible spectrum. This is exactly what is illustrated in Figure 4 of Burlaga et al. (2018), which shows that the compressible spectrum corresponding to Interval 1 and the incompressible spectrum of Interval 2 are virtually identical and overlay one another.

3. Conclusions and Discussion

Based on the surprising magnetic field observations made by *Voyager 1* in the VLISM (Burlaga et al. 2015, 2018), an interesting story about turbulence in the VLISM surrounding the heliosphere is beginning to emerge. In a quiet Interval 1, located between ~2–7 au upwind of the heliopause, the dominant magnetic fluctuations observed in the wavenumber range 1.3×10^{-13}–4×10^{-12} cm^{-1} were parallel to the mean magnetic field (and hence compressive) with a Kolmogorov-like spectrum $\propto k^{-5/3}$. The electron density spectrum derived by Lee & Lee (2019) was also Kolmogorov-like over the corresponding wavenumber scales and smaller (up to ~15 au). Further from the heliopause in a second quiet Interval 2, located between ~9–14 au upwind of the heliopause, the dominant fluctuations were observed to now be transverse to the mean magnetic field, and fluctuations with $\delta B_{\parallel}$ were virtually undetectable. Remarkably, the magnetic PSD over the same range of wavenumbers was essentially identical in amplitude and slope with the compressible spectrum of Interval 1.

In Zank et al. (2017b), we showed that only compressible fast magnetosonic waves could be transmitted from the "compressible reservoir" of the inner heliosheath, across the heliopause, into the VLISM. Neither slow mode nor Alfvén modes can be transmitted. This result has since been supported by the PIC simulations of Matsukiyo et al. (2019). Furthermore, the transmission of the observed $k^{-5/3}$ spectrum of compressible turbulence (Burlaga & Ness 2009, 2010, 2012; Gutynska et al. 2010) from the inner heliosheath was shown to result in a $k^{-5/3}$ spectrum of fast magnetosonic modes in the VLISM (Zank et al. 2017b). In this regard, the turbulence observed by *Voyager 1* close to the heliopause in the VLISM was heliospheric in origin. In this work, we have demonstrated that fast magnetosonic modes in the $\beta_p \ll 1$ VLISM plasma undergo mode conversion via two possible nonlinear three-wave interactions: a fast mode plus a zero-frequency mode yields a slow magnetosonic wave, or a fast mode plus a zero-frequency mode yields an Alfvén wave. The former case gives a very short wavelength slow mode and requires a large $k_{\perp}$ 2D mode, and of course there is no conversion of $\delta B_{\parallel}$ to transverse fluctuations. By contrast, the latter three-wave interaction converts the compressible fast magnetosonic mode to a transverse mode (an Alfvén wave) together with the zero-frequency mode (also possessing only $\delta \boldsymbol{B}_{\perp}$). The Alfvén mode possesses almost the same wavenumber as the initial fast mode. Consequently, the new PSD derived from the conversion of fast magnetosonic waves to Alfvén waves is essentially identical to that of the preceding spectrum.

The compressibility of the fluctuations has been considered further by Fraternale et al. (2019), and they show that the fraction of compressible energy reaches about 50% for frequencies greater than 10^{-5} Hz. However, as we discussed above, it is unclear whether higher frequencies are really more compressible, since the results of Fraternale et al. (2019) use the trace of the PSD of $\boldsymbol{B}$ as a proxy for the density fluctuations that cannot be measured by *Voyager 1*. This will need to be re-examined using *Voyager 2* VLISM observations. For the present, we note that the resonant mode process that generates a slow magnetosonic mode will yield compressible fluctuations with the same frequency but a larger wavenumber than the pump fast magnetosonic mode. This will leave the frequency spectrum unchanged but the wavenumber spectrum will be modified.

The picture that emerges is illustrated in Figure 1, which shows the upwind heliosphere surrounded by a relatively narrow region of compressible (fast magnetosonic waves) turbulence through which *Voyager 1* traversed, passing then through a region of mode conversion to eventually enter a region of properly incompressible turbulence. Nonetheless, despite being incompressible, the observed turbulence is of heliospheric origin, and is therefore superimposed atop the spectrum of (possibly local) (L)ISM turbulence. It is not obvious to us how this paradigm may or may not modify the inferred electron density spectrum presented by Lee & Lee (2019) given that their smaller k spectra are derived by integrating spatially over both the compressible and incompressible regimes.

A very crude estimate suggests that the distance at which Burlaga et al. (2018) observed the transition from compressible to incompressible turbulence is consistent with a mode-coupling timescale. Suppose that the mode-coupling timescale

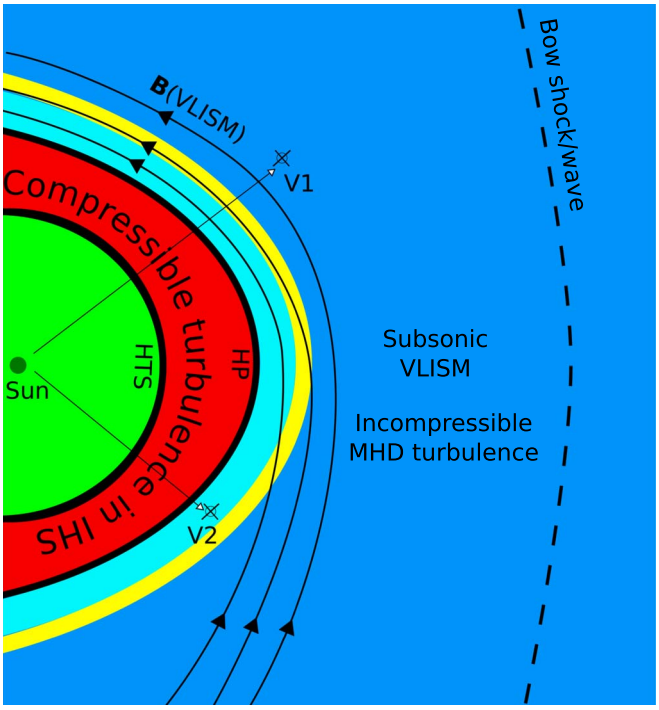

Figure 1. Cartoon showing the general structure of the heliospheric interaction with the local interstellar medium. The heliospheric termination shock (HTS), inner heliosheath (IHS), heliopause (HP), the VLISM, the draping VLISM magnetic field B (VLISM), and a possible bow wave/shock are all identified, as are the *Voyager 1* (V1) and *Voyager 2* (V2) trajectories. The supersonic solar wind is colored green, and the hot IHS red. Compressible turbulence dominates in the IHS. Immediately beyond the HP in the VLISM, colored by a light blue, is a region of compressible (fast magnetosonic modes) turbulence transmitted from the IHS. The yellow band is a region in which mode conversion dominates as magnetosonic waves engage in a nonlinear three-wave interaction with zero-frequency modes to generate incompressible Alfvén waves. The darker blue region associated with the subsonic VLISM is now comprised of incompressible turbulence—a superposition of the mode-converted now incompressible turbulence of heliospheric origin and turbulence associated with the (possibly local) ISM. This cartoon neglects the possible dynamical contribution to low-frequency turbulence by shocks in the VLISM.

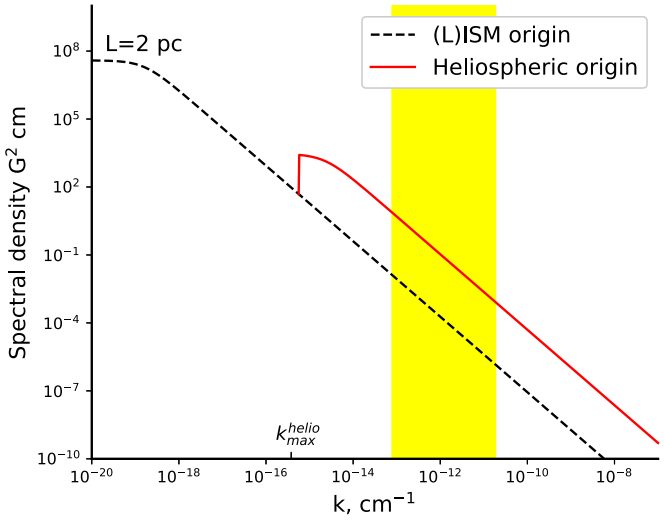

Figure 2. Illustration of the expected form of the incompressible VLISM power spectral density for transverse magnetic field fluctuations. A background interstellar spectrum of the form $G(k) = (5\sin(3\pi/5)/6\pi)[\langle\delta\hat{B}^2\rangle L/(1+(kL)^{5/3})]$ (Giacalone & Jokipii 1999; Zank 2014) is assumed and $L = 2$ pc is prescribed (Burlaga et al. 2015; Zank et al. 2017b; Burlaga et al. 2018), to which is added the incompressible spectrum of heliospheric origin. The spectral amplitude of the heliospheric component corresponds to that observed (see Figure 4 of Burlaga et al. 2018) and the compressible spectrum derived in Zank et al. (2017b; their Figure 8). In extending the spectrum of heliospheric origin to smaller k values, we used a correlation length $\ell_c = 4.5 \times 10^9$ km in the functional form above (Giacalone & Jokipii 1999; Zank 2014), and assumed that the maximum k value, $k_{\rm max}^{\rm helio}$, was given by a crude scaling with the size of the heliopause, $2\pi \times 120$ au. The k band over which the *Voyager 1* observations were made corresponds to the yellow shading.

τ_m can be estimated crudely from the zero-frequency (τ_0) and fast mode wave (τ_f) timescales according to $\tau_m^{-1} \lesssim \tau_0^{-1} + \tau_f^{-1}$. If we let ℓ be a characteristic length scale, so that $k = 2\pi\,\ell^{-1}$, and suppose that the nonlinear timescale $\tau_0^{-1} \sim \ell^{-1}\langle z^{\infty\pm 2}\rangle^{1/2}$ (Zank et al. 2017a) can be approximated as $\ell^{-1}0.1|U|$ ($|U|$ the VLISM flow speed) in the NI MHD approximation, then the mode-coupling timescale can be approximated in the $\beta_p \ll 1$ limit as $\tau_m^{-1} \lesssim \ell^{-1}(0.1)|U| + \ell^{-1}(V_A - |U|)$ (after Doppler-shifting the fast mode propagating into the oncoming flow). Burlaga et al. (2013) suggest a flow speed of $|U| \sim 20\,\mathrm{km\,s^{-1}}$ and Alfvén speed $V_A \sim 38\,\mathrm{km\,s^{-1}}$, from which one obtains $\tau_m^{-1} \lesssim 3.2 \times 10^5 k\ \mathrm{s^{-1}}$ for wavenumber k measured in $\mathrm{cm^{-1}}$. For the wavenumber interval observed by Burlaga et al. (2015, 2018), $k \in (10^{-12},\ 10^{-13})\,\mathrm{cm^{-1}}$, choosing $\tau_m^{-1} \sim 10^5 k\ \mathrm{s^{-1}}$ yields $\tau_m \sim 10^7$–10^8 s, i.e., this τ_m approximates crudely the nonlinear mode-coupling timescale for the three-wave interaction of Alfvén—fast magnetosonic—zero-frequency modes over the wavenumber range of $\sim 10^{-12}$–$10^{-13}\,\mathrm{cm^{-1}}$. The mode-coupling timescale yields a characteristic distance range from the heliopause over which compressible fast magnetosonic waves can propagate into the oncoming VLISM flow before converting to an Alfvén or zero-frequency mode. On assuming a propagation speed of $\sim 20\,\mathrm{km\,s^{-1}}$ into the oncoming VLISM flow, we find $L \sim 20 \times 10^7$–10^8 km $\gtrsim$1–10 au from the heliopause. Hence, we would expect that beyond $\sim$10 au from the heliopause, compressible fluctuations in the 10^{-12}–$10^{-13}\,\mathrm{cm^{-1}}$ wavenumber range transmitted from the inner heliosheath, across the heliopause, into the VLISM will have been fully mode-converted to incompressible fluctuations. Interval 2 was located between 9 and 14 au upwind of the heliopause.

Since Interval 2 was from 9 to 14 au from the heliopause, let us suppose that a distance $\sim$15 au from the heliopause identifies the incompressible region of the VLISM. In this region, the turbulent interaction timescale can be estimated as (Matthaeus & Zhou 1989; Zank et al. 2017a)

$$\tau_t^{-1} = \tau_0^{-1} + \tau_A^{-1}, \tag{29}$$

where τ_0 is the nonlinear timescale defined above and $\tau_A^{-1} = \ell^{-1}V_A$ is the (inverse) Alfvén timescale. As above, we approximate $\langle z^{\infty\pm 2}\rangle^{1/2}$ by $0.1|U|$. To find the largest scale that will experience an "eddy turnover" (which will yield an estimate for the correlation length), we equate the turbulent interaction timescale τ_t with the time T taken for a magnetic field line to advect 15 au i.e., $T \simeq 15$ au $/U$. From (29), we find that $\ell_c \sim 4.5 \times 10^9$ km (i.e., $\sim$30 au) or $k_c \equiv 2\pi/\ell_c = 1.4 \times 10^{-14}\,\mathrm{cm^{-1}}$.

If we take the view advocated here and in Zank et al. (2017b), that the turbulence observed in both Intervals 1 and 2 is of heliospheric origin, then one can reasonably suppose that the observed spectrum is superimposed on the (L)ISM spectrum of magnetic field fluctuations. In that case, the PSD should have the form illustrated in Figure 2 rather than that shown in Figure 4 of Burlaga et al. (2018). The extent of the superimposed PSD of

heliospheric origin will be bounded by the largest-scale (smallest $k_{\max}^{\rm helio}$) magnetosonic mode that can be transmitted from the inner heliosheath into the VLISM. This is likely to be a scale on the order of some fraction of the size of the heliopause in the upwind direction, i.e., some fraction of $2\pi\ R_{HP} \sim 2\pi \times 120$ au. It was pointed out by the referee that both solar rotation and the solar cycle may act to drive the largest scales of heliospheric turbulence in the VLISM. One can use $k = 2\pi f/|V_A - U|$, where f is the frequency, and $\sim|V_A - U|$ is the propagation speed for fast magnetosonic waves to show that the solar rotation frequency $f_{sr} \simeq 4.5 \times 10^{-7}$ Hz yields $k_{sr} \simeq [7.6 \times 10^{-13}, 1.6 \times 10^{-12}]\,{\rm cm}^{-1}$ for $U = [0.20]\,{\rm km\,s}^{-1}$, respectively. Similarly, using the solar cycle periodicity $f_{sc} \simeq 3 \times 10^{-9}$ Hz yields $k_{sc} \simeq [5 \times 10^{-15}, 10^{-14}]\,{\rm cm}^{-1}$. These latter values are comparable to the wavenumber of $k_{\max}^{\rm helio}$. Simulations of the interaction of a solar wind whose ram pressure varies with solar cycle and the LISM (Zank & Müller 2003; Washimi et al. 2017) show that the heliopause moves outward and inward asynchronously with the solar cycle, driving enormous global heliospheric pressure waves and rarefactions into the VLISM.

As discussed in Zank et al. (2017b), the smallest transmitted fluctuations may be on the order of ∼0.02 au or less (see also Matsukiyo et al. 2019). The energy spectrum will then cascade to larger values of k than the minimum injected value from the inner heliosheath. The effect of injecting energy into the turbulence spectrum at wavenumbers greater than $k_{\max}^{\rm helio}$ is to generate a new correlation length or outer scale. Such a possibly weak enhancement of the interstellar spectrum might be observed on scales of ∼100 au and less. We note that the small wavenumber component of heliospheric origin is likely to be compressible at much larger distances from the heliopause than Interval 2 because the mode conversion timescale is inversely proportional to k.

In the case of superimposed spectra of heliosheath and (L) ISM origin, as illustrated in Figure 2, one would expect the outer scale to be larger than the ∼2000 au (or ∼0.01 pc) suggested by Burlaga et al. (2018). Their estimate was based on an extrapolation of the level of the VLISM turbulence observed by *Voyager 1*, using the expression for the interstellar magnetic PSD introduced by Giacalone & Jokipii (1999). If instead the turbulence of heliospheric origin is an order of magnitude larger than the (L)ISM turbulence in the corresponding wavenumber range, then the outer scale L is significantly larger than 0.01 pc, being given by $L \simeq 2$ pc as illustrated in Figure 2. This is of course simply a guess regarding the (L)ISM turbulence parameters, but it may be supported indirectly by the very small values of $\delta \boldsymbol{B}_{\perp}$ barely detected in Interval 1 by Burlaga et al. (2015). A better extrapolation for the (L)ISM magnetic PSD would be to measure the transverse fluctuations in Interval 1 to determine their spectral intensity. Unfortunately, as emphasized by Burlaga et al. (2018), measurements of magnetic field fluctuations in the VLISM are extremely difficult, being so close to the noise threshold of the *Voyager 1* magnetometer. Nevertheless, further measurements by *Voyager 1* and 2, the latter of which will include plasma data, will provide further insights into this fascinating problem.

Before concluding, we discuss briefly one further interesting possibility for the generation and possible enhancement of VLISM turbulence. Fraternale et al. (2019) suggest that the observed VLISM shocks of solar origin (Zank & Müller 2003; Gurnett et al. 2013, 2015; Kim et al. 2017; Mostafavi & Zank 2018) may lead to wave-scattering and processing of VLISM turbulence, although no model is proposed. A possible difficulty with the shock-induced wave-scattering idea is the weakness of the observed VLISM shocks and their remarkable thickness (Gurnett et al. 2013, 2015), which has been ascribed to their being collisional shocks and the structure being determined by thermal proton–proton collisions (Mostafavi & Zank 2018). Based on prior models of the interaction of turbulence with shocks (e.g., McKenzie & Westphal 1968), it seems unlikely that simple transmission of VLISM turbulence across a very weak shock will generate significant levels of MHD turbulence. It is interesting, however, that if turbulence were generated by this mechanism, it would likely be dominated by compressible fluctuations rather than transverse magnetic field fluctuations (McKenzie & Westphal 1968). However, it is instructive to note that Gurnett et al. (2015) proposed a model of a weak quasi-perpendicular VLISM shock that reflected incident galactic cosmic rays to form a beam streaming away upstream from the shock (see their Figure 7). Such a beam will of course be subject to a streaming instability (e.g., Gordon et al. 1999; Rice et al. 2003) and be unstable to the generation of Alfvén waves. This may well be a further mechanism for exciting low-frequency turbulence in the VLISM and may distinguish the quiet intervals investigated by Burlaga et al. (2015, 2018) and Fraternale et al. (2019) from the shock-influenced regions that were considered also by Fraternale et al. (2019). The possibility of a shock source of turbulence should be considered in further studies of turbulence in the VLISM, since this may increase the amplitude of the observed turbulence farther from the heliopause. The additional generation of turbulence by VLISM shocks might be of particular importance, since Fraternale et al. (2019) suggest that the nature of the magnetic field fluctuations does not change continuously from the HP(∼122 au) to ∼140 au, whereas for a pristine VLISM, one would expect that the wave conversion mechanism proposed here would lead to a relatively continuous change from compressible to incompressible turbulence with increasing distance. The addition of shock-excited turbulence may therefore provide a very natural explanation for this observation.

Finally, we note that despite being a rather ordinary G-class star embedded in a warm ISM, the Sun may provide an interesting astronomical example for the manner in which turbulence associated with the inner asterosheath (i.e., the region between the stellar wind termination shock and the asteropause) of other stars may lead to the transmission of compressible turbulence into the surrounding very local circumstellar ISM, which will then be mode-converted to incompressible fluctuations in the ISM. This appears to be a novel manner in which stars inject turbulence into the ISM on scales that depend on the size of the asteropause and with an effectiveness that depends on the level of compressible turbulence in the inner asterosheath, which depends in turn on the level of stellar activity.

We acknowledge the partial support of an NSF EPSCoR RII-Track-1 Cooperative Agreement OIA-1655280, and partial support from an NSF/DOE Partnership in Basic Plasma Science and Engineering via NSF grant PHY-1707247, and a NASA *IBEX* grant Sub0000167/80NSSC18K0237.

ORCID iDs

G. P. Zank https://orcid.org/0000-0002-4642-6192
M. Nakanotani https://orcid.org/0000-0002-7203-0730
G. M. Webb https://orcid.org/0000-0002-0617-9502

References

Adhikari, L., Khabarova, O., Zank, G. P., & Zhao, L. L. 2019, ApJ, 873, 72
Adhikari, L., Zank, G. P., Hunana, P., et al. 2017a, ApJ, 841, 85
Adhikari, L., Zank, G. P., Telloni, D., et al. 2017b, ApJ, 851, 117
Alexandrova, O. 2008, NPGeo, 15, 95
Avinash, K., Zank, G. P., Dasgupta, B., & Bhadoria, S. 2014, ApJ, 791, 102
Bieber, J. W., Matthaeus, W. H., Smith, C. W., et al. 1994, ApJ, 420, 294
Bieber, J. W., Wanner, W., & Matthaeus, W. H. 1996, JGR, 101, 2511
Borovikov, S. N., & Pogorelov, N. V. 2014, ApJL, 783, L16
Borovikov, S. N., Pogorelov, N. V., Zank, G. P., & Kryukov, I. A. 2008, ApJ, 682, 1404
Burlaga, L. F., Florinski, V., & Ness, N. F. 2015, ApJL, 804, L31
Burlaga, L. F., Florinski, V., & Ness, N. F. 2018, ApJ, 854, 20
Burlaga, L. F., & Ness, N. F. 2009, ApJ, 703, 311
Burlaga, L. F., & Ness, N. F. 2010, ApJ, 725, 1306
Burlaga, L. F., & Ness, N. F. 2012, ApJ, 744, 51
Burlaga, L. F., Ness, N. F., & Acuña, M. H. 2006, ApJ, 642, 584
Burlaga, L. F., Ness, N. F., Gurnett, D. A., & Kurth, W. S. 2013, ApJL, 778, L3
Florinski, V., Zank, G. P., & Pogorelov, N. V. 2005, JGRA, 110, A07104
Fraternale, F., Pogorelov, N. V., Richardson, J. D., & Tordella, D. 2019, ApJ, 872, 40
Galtier, S., Nazarenko, S. V., & Newell, A. C. 2001, NPGeo, 8, 141
Giacalone, J., & Jokipii, J. R. 1999, ApJ, 520, 204
Gordon, B. E., Lee, M. A., Möbius, E., & Trattner, K. J. 1999, JGR, 104, 28263
Gurnett, D. A., Kurth, W. S., Burlaga, L. F., & Ness, N. F. 2013, Sci, 341, 150
Gurnett, D. A., Kurth, W. S., Stone, E. C., et al. 2015, ApJ, 809, 121
Gutynska, O., Šafránková, J., Němeček, Z., & Richardson, J. D. 2010, ApJL, 722, L228
Hunana, P., & Zank, G. P. 2010, ApJ, 718, 148
Kadomtsev, B. B., & Pogutse, O. P. 1973, ZhETF, 65, 575
Khabarova, O., Zank, G. P., Li, G., et al. 2015a, ApJ, 808, 181
Khabarova, O. V., & Zank, G. P. 2017, ApJ, 843, 4
Khabarova, O. V., Zank, G. P., Li, G., et al. 2015b, JPhCS, 642, 012033
Khabarova, O. V., Zank, G. P., Li, G., et al. 2016, ApJ, 827, 122
Khabarova, O. V., Zank, G. P., Malandraki, O. E., et al. 2017, SunGe, 12, 23
Kim, T. K., Pogorelov, N. V., & Burlaga, L. F. 2017, ApJL, 843, L32
Klainerman, S., & Majda, A. 1981, CPAM, 34, 481
Klainerman, S., & Majda, A. 1982, CPAM, 35, 629
Kuznetsov, E. A. 2001, JETP, 93, 1052
Lee, K. H., & Lee, L. C. 2019, NatAs, 3, 154
Lighthill, M. J. 1960, RSPTA, 252, 397
Lion, S., Alexandrova, O., & Zaslavsky, A. 2016, ApJ, 824, 47
Matsukiyo, S. T., Noumi, T., Zank, G., Washimi, H., & Hada, T. 2019, ApJ, in press
Matthaeus, W. H., Klein, L. W., Ghosh, S., & Brown, M. R. 1991, JGR, 96, 5421
Matthaeus, W. H., & Zhou, Y. 1989, PhFlB, 1, 1929
McKenzie, J. F., & Westphal, K. O. 1968, PhFl, 11, 2350
Mostafavi, P., & Zank, G. P. 2018, ApJL, 854, L15
Perrone, D., Alexandrova, O., Mangeney, A., et al. 2016, ApJ, 826, 196
Perrone, D., Alexandrova, O., Roberts, O. W., et al. 2017, ApJ, 849, 49
Pogorelov, N. V., Heerikhuisen, J., Roytershteyn, V., et al. 2017, ApJ, 845, 9
Rice, W. K. M., Zank, G. P., & Li, G. 2003, JGRA, 108, 1369
Roberts, D. A., Klein, L. W., Goldstein, M. L., & Matthaeus, W. H. 1987, JGR, 92, 11021
Shebalin, J. V., Matthaeus, W. H., & Montgomery, D. 1983, JPlPh, 29, 525
Telloni, D., Perri, S., Bruno, R., Carbone, V., & Amicis, R. D. 2013, ApJ, 776, 3
Verkhoglyadova, O. P., Dasgupta, B., & Tsurutani, B. T. 2003, NPGeo, 10, 335
Washimi, H., Tanaka, T., & Zank, G. P. 2017, ApJL, 846, L9
Webb, G. M., Zakharian, A., Brio, M., & Zank, G. P. 1999, JPlPh, 61, 295
Webb, G. M., Zakharian, A. R., Brio, M., & Zank, G. P. 2000, JPlPh, 63, 393
Webb, G. M., Zakharian, A. R., Brio, M., & Zank, G. P. 2001, JPlPh, 66, 167
Zank, G. P. 1999a, SSRv, 89, 413
Zank, G. P. 1999b, in AIP Conf. Proc. 471, The Solar Wind Nine Conference, ed. S. R. Habbal & C. D. Halas (Melville, NY: AIP), 783
Zank, G. P. 2014, Transport Processes in Space Physics and Astrophysics, Vol. 877 (Berlin: Springer)
Zank, G. P. 2015, ARA&A, 53, 449
Zank, G. P., Adhikari, L., Hunana, P., et al. 2017a, ApJ, 835, 147
Zank, G. P., Adhikari, L., Zhao, L. L., et al. 2018, ApJ, 869, 23
Zank, G. P., Du, S., & Hunana, P. 2017b, ApJ, 842, 114
Zank, G. P., Heerikhuisen, J., Wood, B. E., et al. 2013, ApJ, 763, 20
Zank, G. P., & Matthaeus, W. H. 1992a, JPlPh, 48, 85
Zank, G. P., & Matthaeus, W. H. 1992b, JGR, 97, 17189
Zank, G. P., & Matthaeus, W. H. 1993, PhFl, 5, 257
Zank, G. P., & Müller, H.-R. 2003, JGRA, 108, 1240
Zank, G. P., Pauls, H. L., Williams, L. L., & Hall, D. T. 1996, JGR, 101, 21639
Zhao, L. L., Adhikari, L., Zank, G. P., Hu, Q., & Feng, X. S. 2018a, ApJ, 856, 94
Zhao, L. L., Zank, G. P., Chen, Y., et al. 2019, ApJ, 872, 4
Zhao, L. L., Zank, G. P., Khabarova, O., et al. 2018b, ApJL, 864, L34
Zhou, Y., Matthaeus, W. H., & Dmitruk, P. 2004, RvMP, 76, 1015